

Alma Mater Studiorum Università di Bologna  
Archivio istituzionale della ricerca

The competition between dehydrogenation and dehydration reactions for primary and secondary alcohols over gallia: unravelling the effects of molecular and electronic structure via a two-pronged theoretical/experimental approach.

This is the final peer-reviewed author's accepted manuscript (postprint) of the following publication:

*Published Version:*

L. Izzo, T.T. (2020). The competition between dehydrogenation and dehydration reactions for primary and secondary alcohols over gallia: unravelling the effects of molecular and electronic structure via a two-pronged theoretical/experimental approach. CATALYSIS SCIENCE & TECHNOLOGY, 10, 3433-3449 [10.1039/c9cy02603g].

*Availability:*

This version is available at: <https://hdl.handle.net/11585/787427> since: 2023-04-23

*Published:*

DOI: <http://doi.org/10.1039/c9cy02603g>

*Terms of use:*

Some rights reserved. The terms and conditions for the reuse of this version of the manuscript are specified in the publishing policy. For all terms of use and more information see the publisher's website.

This item was downloaded from IRIS Università di Bologna (<https://cris.unibo.it/>).  
When citing, please refer to the published version.

(Article begins on next page)

This is the final peer-reviewed accepted manuscript of:

**Lorella Izzo, Tommaso Tabanelli, Fabrizio Cavani, Paola Blair Vàsquez, Carlo Lucarelli, Massimo Mella, “The competition between dehydrogenation and dehydration reactions for primary and secondary alcohols over gallia: unravelling the effects of molecular and electronic structure via a two-pronged theoretical/experimental approach”, Catal. Sci. Technol., 2020, 10, 3433–3449**

The final published version is available online at:  
<https://doi.org/10.1039/C9CY02603G>

Terms of use:

Some rights reserved. The terms and conditions for the reuse of this version of the manuscript are specified in the publishing policy. For all terms of use and more information see the publisher's website.

*This item was downloaded from IRIS Università di Bologna (<https://cris.unibo.it/>)*

***When citing, please refer to the published version.***

# **The competition between dehydrogenation and dehydration reactions for primary and secondary alcohols over gallia: unravelling the effects of molecular and electronic structure via a two-pronged theoretical/experimental approach**

*Lorella Izzo<sup>a</sup>, Tommaso Tabanelli<sup>b</sup>, Fabrizio Cavani<sup>b,c</sup>, Paola Blair Vàsquez<sup>b</sup>, Carlo*

*Lucarelli<sup>d,c\*</sup>, Massimo Mella<sup>d\*</sup>*

<sup>a</sup>Dipartimento di Biotecnologia e Scienze della Vita, Università degli Studi dell'Insubria, via J.

H. Dunant 3, 21100 Varese (I)

<sup>b</sup>Dipartimento di Chimica Industriale “Toso Montanari”, Università degli Studi di Bologna,

Viale Risorgimento 4, 40136 Bologna (I)

<sup>c</sup>Consorzio INSTM, Research Unit of Bologna, Florence

<sup>d</sup>Dipartimento di Scienza ed Alta Tecnologia, Università degli Studi dell'Insubria, via Valleggio

11, 22100 Como (I)

Acid oxides, dehydration, dehydrogenation, electronic structure calculations, catalytic test, in situ spectroscopy.

To explore alternative applications of gallium (III) oxide and co-precipitated Ga(III)/M(II) oxides (M=Mg, Ca, and Sr), we investigate the relative dehydrogenation/dehydration activity of nanostructured gallia on alcohols via electronic structure calculations, reactivity tests and DRIFT-IR spectroscopy. Computing relative reaction barriers with all electron DFT and split-valence basis sets on a panel of 11 alcohols suggested dehydrogenation to be the most active process catalyzed by gallia for both primary and secondary alcohols despite its fundamentally acid behavior, which

was previously suggested to foster dehydration. A key contribution in defining the most active channel is also provided by the interaction between the alcohol carbon skeleton and gallia surface. The only deviation from the relative reactivity just discussed is found for 1-phenyl ethanol, an outcome easily rationalized by the conjugated nature of the nearly-carbocation TS leading to styrene. Catalytic tests on methanol, ethanol, 1- and 2-propanol at 400 °C supported the proposed relative selectivity; besides, the recorded alcohol total conversions and product yields agree well with what proposed by the DFT reaction profiles, thus demonstrating the predictive capability of the chosen electronic structure approach. Finally, temperature programmed DRIFT spectroscopy on the aliphatic C3 alcohols was able to characterize the adsorbed reactants, intermediates, and products, fully supporting the picture described by the theoretical modelling and the reactivity tests. In conclusion, the lower acidity of Ga(III), due to its semi-metallic nature and its larger ionic radius, compared to Al(III) leads to opposite selectivity in the competition between alcohol dehydrogenation and dehydration at 400 °C, the oxide of the latter ion being known to preferentially produce olefins.

## Introduction

With short alcohols possibly being produced from renewable feedstocks, processes able to convert them in more useful chemicals or to exploit them as useful reactants are uninterruptedly sought. As a few examples, we mention their upgrading to higher mass alcohols via Guerbet-type reactions[1][2], the production of short chain olefins[3][4]–[7][4], [8], [9], [9] or dienes[1], as reducing agents via MPV-type processes[10][10][11][12][13], or for the direct alkylation of activated aromatic compounds[14][14][15][16][17][18][19][20][21][22].

When heterogeneously catalysed, a few of the processes mentioned require the *in-situ* production of carbonylic compounds (i.e. aldehydes and ketones), whose higher (and different) reactivity compared to the alcoholic one is key in obtaining the sought high value products. In this respect, the case represented by the direct methylation of phenols from methanol requires the activation of the latter via its partial oxidation to formaldehyde. Compared to pure MgO, Ga(III)[14] or Fe(III)[18]-doped MgO performance in phenol methylation are highly improved due to a more facile formation of formaldehyde, suggesting that the trivalent ions are able to foster methanol

dehydrogenation. This was indeed demonstrated by direct exploration of the methanol chemistry over such mixed materials, with an interesting effect on the selectivity toward 2,4,6-trimethyl phenol due to the co-feeding of water steam together with methanol and phenol on mixed Mg/Ga oxide with a 10:1 molar ratio for the two cations[14]. Interestingly, also gallia demonstrated the ability of methylating phenol in conditions similar to the ones employed for the mixed oxides, indicating the capability of both dehydrogenating methanol and of activating phenols[14].

In principle, the ability of gallia (and, likely, of Ga(III) in mixed oxides) to dehydrogenate secondary alcohols was evidence previously for 2-propanol[23][24], and it could be exploited to alkylate aromatic compounds with heavier alkyl groups. On the other hand, if the dehydration process takes place preferentially, as suggested to happen for secondary alcohols in milder conditions[25], the produced olefins may quickly desorb from the catalyst surface or be condensed with the alcohol producing ethers[9]. In all cases, the reactivity typical of the carbonyl group may not be at our disposal, as it happens for ethanol over  $\gamma$ -Al<sub>2</sub>O<sub>3</sub>, with the mentioned reactive channels being markedly preferred compared to dehydrogenation[5], [6], [9], [26]. This latter behaviour was correctly modelled via a Al<sub>6</sub>O<sub>9</sub> cluster representing the tri-coordinated Al(III) site and surrounding di- and tri-coordinated oxygen atoms[27][5], [9][4][4] and attributed to the cation acidity; indeed, the barrier to be surmounted in an E2 -type reaction to produce an olefin on the same catalyst decreases upon increasing the substitution or alkyl chain length of aliphatic alcohols, as predicted by electronic structure modeling[8]. The same trend for the E2 activation barrier seems to be present also when isomorphic gallia or indium (i.e. with metal atoms showing similar coordination numbers, hence activity, as Al(III) in alumina[28][29][30][31][32][33]) are employed, albeit the barriers are 2.5-5 kcal/mol higher than for alumina, and they decrease less quickly upon increasing alcohol substitution on indium[8]. Besides, the substitution of the tri-

coordinated Al(III) in the putative active site with either Ga(III) or In(III) raises the energetic location of the transition state (TS) despite the surrounding environment is left unchanged, so that the barriers are quite similar to the ones obtained with pure gallia or indium when the tri-coordinated oxygen is employed as basic site. This latter finding suggests that the electronic structure of the cation on the active site markedly modulates the catalyst activity, making it substantially independent of the local environment.

From what just discussed, one may wonder whether the higher E2 barriers computed in Ref. [8] for gallia could lead to a different reactivity of alcohols heavier than methanol previously suggested by catalytic tests on 2-propanol[23], [24]. As indicated, one may be particularly interested in generating aldehydes from primary alcohols and ketones from secondary ones in order to alkylate aromatic compounds. *De facto*, albeit earlier tests of the reactivity of secondary alcohols heavier than 2-propanol on gallia suggested the principal product to be olefins[25], with a selectivity depending on the way the catalyst is prepared and the reaction conducted[23], even the possibility of dehydrogenating primary alcohols could, in principle, be used advantageously for further transformations. Interestingly, we were not able to find previous published work on the matter and considered the topic worth of investigation; we thus decided to better characterize the possible catalytic behavior of pure gallia. Our motivations derive also from the observation that the electronic structure results of ethanol reactivity on  $\gamma$ -Al<sub>2</sub>O<sub>3</sub> by Dixon and co-workers[27] indicated that barriers height between dehydration and dehydrogenation differ by, at most, 4 kcal/mol, so that selectivity may be tuned by modifications induced in the catalyst relative acidity/basicity. We thus feel that an in-depth investigation of the competition between the latter two processes on gallia is indeed worth, and we tackle such task exploiting theoretical modeling, direct reactivity tests, as well as DRIFT spectroscopy on a relevant set of alcohols.

The organization of this paper is as follow. In Section 2, we describe all the methodologies employed in this multi-faceted work. Section 3 reports on the theoretical and experimental results obtained in our work, providing also a discussion and rationalization for them. For the sake of clarity, and to somewhat represent the chronological evolution of the results, we discuss initially the reactivity of the two lightest alcohols (methanol and ethanol) to shed some light on the general properties of the studied systems. Changes in the reactivity/selectivity induced by modification of the primary/secondary nature of the alcohol, as well as the chain length, would successively be discussed exploiting 1- and 2-propanol, two species suitable for the analysis of their reaction products via an on-line micro GC downstream the reactor tube. The latter two alcohols have also been employed for *in situ* DRIFT spectroscopic experiments, with the goal of better characterizing the adsorbed species and their evolution with respect to temperature. Finally, the presentation of our results is completed by discussing the quantitative structure-properties relationship emerging from electronic structure calculations on six additional alcohols including longer chain aliphatic species, as well as unsaturated or aromatic substituted methanol and ethanol. The last Section provides our conclusions and indications on avenues of future exploration.

## **Methodologies**

### **1.Theoretical modelling**

Gas-phase electronic structure calculations were carried out using the Gaussian09 suites of codes and the B3LYP[34], [35] density functional theory (DFT), including all the electrons in the calculations. The basis set used was 6-31+G(d,p). This level of description can be shown to be an excellent compromise between computational costs and accuracy by comparing with CCSD(T) results[27]. To model adsorption and reactivity of alcoholic species on pristine  $\text{Ga}_2\text{O}_3$ , we exploited a cluster approach used to rationalise differences in reactivity between  $\text{Al}_2\text{O}_3$ ,  $\text{Ga}_2\text{O}_3$ ,

and  $\text{In}_2\text{O}_3$  [4], [8], [9], as well as the impact of water steam on phenol adsorption[14]. A  $(\text{Ga}_2\text{O}_3)_4$  aggregate was used to model the adsorption of oxygenated molecules onto a tri-coordinated surface  $\text{Ga}^{3+}$  ion and their subsequent transformations; the size of the aggregate appeared sufficiently large to limit possible polarisation effects due to the edge vicinity. Given the limited size of our molecular models, it was also possible to allow the full relaxation of the model crystal in order to investigate the presence of strain effects, to compute vibrational frequencies for the sake of comparison with DRIFT spectra, and to estimate correctly energy profile as light species such as hydrogen are exchanged between system fragments. Putative structures for energy minima were built using data from previous works by us[14] and others[8], [27], a step followed by a complete geometrical relaxation of the adsorbed species while keeping the oxide cluster constrained. The latter moiety was subsequently relaxed with no constraints on all coordinates. In general, the cluster representing gallia initially maintained its original relative disposition of the atoms closely resembling pristine gallia structure with or without the presence of adsorbed species. Slight distortion of the coordination geometry for one of the three oxygen atoms bound to the vertex (active site)  $\text{Ga(III)}$  has, however, been observed during the optimization of TS's; such structural modification invariably lead to somewhat lower lying stationary points, so that we employed it in all our calculations. Considering that the pure gallia cluster lowers its energy by 6.8 kcal/mol upon buckling, employing as the definition of energy zero a cluster with unbuckled structure requires adding to the energy profiles -6.8 kcal/mol.

## **2. Reactivity tests**

Alcohols decomposition over  $\text{Ga}_2\text{O}_3$ , have been investigated in a continuous-flow, gas-phase, fixed-bed micro-reactor (Pyrex, tubular glass reactor) with a length of 450 mm and an inner diameter of 19 mm[14], [36][37]. The liquid alcohols (methanol, ethanol, 1-propanol and 2-



propanol, all of them HPLC grade) were fed to a heated line (230°C), directly connected to the reactor, by means of a high precision KD Scientific Legacy Syringe-infusion Pump, obtaining an instant vaporisation in the nitrogen stream (gas carrier). In a typical experiment, the reaction temperature was set to 400°C, methanol (0.0057 mL/min) was fed inside the reactor previously loaded with 1 g of monoclinic Ga<sub>2</sub>O<sub>3</sub> particles (Fig. S1, gallium III oxides 99,99% supplied by Sigma Aldrich, corresponding to around 0.7 cm<sup>3</sup> volume). Nitrogen (15 mL/min) was used both as carrier and diluent for the organic reagent, in order to work with a residence time of 1 second and an alcohol mol% ranging between 12 and 16%. Catalyst particles were previously prepared by pressing the calcined powder into a tablet, which was then crushed over sieves in order to obtain the desired particle size (30-60 mesh, 250-595 µm). Before each test the catalyst was pre-treated in-situ by feeding air inside the reactor at 400°C for 1 hour. Total pressure was atmospheric. The outlet stream from the reactor was directly connected with a heated line (230°C) to an on-line micro GC Agilent 3000A equipped with three different parallel columns for the products quantification: i) Agilent PlotQ column using He as carrier for the separation and quantification of methanol, water, CO<sub>2</sub>, methane, ethylene and propylene; ii) OV1 column using He as carrier for the separation of CO<sub>2</sub>, formaldehyde, diethyl ether, H<sub>2</sub>O, ethanol, 1-propanol, isopropanol and acetone; iii) a molecular sieves column using Ar as carrier for the separation of H<sub>2</sub>, O<sub>2</sub>, N<sub>2</sub>, CH<sub>4</sub>, and CO. In the latter case, a PlotU backflash column was installed to avoid CO<sub>2</sub> and H<sub>2</sub>O poisoning of the stationary phase.

Alcohol conversion and yields of each product were calculated as previously reported in literature[37]. In particular, alcohol conversion and products yields have been calculated by referring the outlet molar flow to the inlet molar flow of the alcohol, normalised by the C atoms, as follow:

$$X_{alcohol} = \frac{\%mol\ alcohol\ in - \%mol\ alcohol\ out}{\%mol\ alcohol\ in} * 100 \quad (1)$$

$$Y_{product\ i} = \frac{\%mol\ i}{\%mol\ alcohol} * \frac{C\ i}{C\ alcohol} * 100 \quad (2)$$

In the case of H<sub>2</sub>O and H<sub>2</sub> the yields have been calculated as follow:

$$Y_{water} = \frac{\%mol\ water}{\%mol\ alcohol} * 100 \quad (3)$$

$$Y_{hydrogen} = \frac{\%mol\ hydrogen}{\%mol\ alcohol} * \frac{2}{H\ atom\ alcohol} * 100 \quad (4)$$

### 3. In Situ DRIFT Spectroscopy

DRIFT spectra were acquired in situ with a Bruker Vertex 70 instrument equipped with a Pike DiffusIR cell attachment. The spectra were recorded using an MCT detector after 128 scans and with a 4 cm<sup>-1</sup> resolution in the region 4000-450 cm<sup>-1</sup>. As a general procedure, a sample of Ga<sub>2</sub>O<sub>3</sub> was loaded and pre-treated at 450 °C under a flow of He (10 mL/min) for 45 min in order to remove any molecules adsorbed onto it. Then, the sample was cooled down to 50 °C. The background was measured, and immediately after, a pulse of 1-propanol or 2-propanol or 2-propanone or propylene or propionaldehyde (1 µL) was introduced. IR spectra were acquired at 0.5 min time intervals to follow the adsorption process. Afterward, the carrier gas was left to flow until the weakly adsorbed probe molecule was evacuated. The IR spectrum acquired after reaching this condition was used to compare the behaviour of the catalysts. The sample was heated till 450°C and spectra were recorded at 50°C interval. The continuous experiments were conducted after catalyst pre-treatment feeding continuously the probed molecule diluted in a He flow at 350°C and spectra were acquired at 0.5 min time intervals[38], [39]. Notice that bands assignment was helped by the results of DFT-based normal model calculations on the investigated species[40].

### 4. Catalyst Characterization

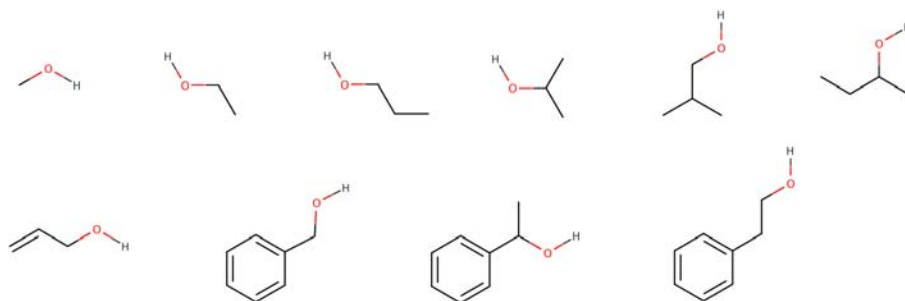
BET, Specific Surface Area. The specific surface area of the catalysts was determined by N<sub>2</sub> absorption–desorption at liquid N<sub>2</sub> temperature using a Sorpty 1750 Fison instrument. 0.35 g of the sample was typically used for the measurement, and the sample was outgassed at 150 °C before N<sub>2</sub> absorption. Results are reported in Table S1 and accompanying text of the ESI.

Temperature-Programmed Desorption (TPD). NH<sub>3</sub> and CO<sub>2</sub>-TPD analyses were performed with a POROTEC Chemisorption TPD/R/O 1100 automated system for analysing the acid/base properties of catalysts. In normal conditions, 0.4g of the fresh catalyst was pre-treated in 10 vol % O<sub>2</sub> in He (30 mL/min of flow rate) to the chosen calcination temperature (10 °C/min to 500 °C for 1 h), in order to remove adsorbed H<sub>2</sub>O and CO<sub>2</sub> from the catalyst surface prior to adsorption. For the exhaust catalyst characterization, the pre-treatment of the catalyst was not performed. The samples were then cooled to 40 and 100 °C for CO<sub>2</sub>-TPD and the NH<sub>3</sub>-TPD analysis, respectively. NH<sub>3</sub> was adsorbed at 100 °C to eliminate the contribution of very weak acid sites and improve the spectrum resolution. The catalyst surface was saturated with the probe molecule for 1 h (flow rate of 30 mL/min of 10 vol % of CO<sub>2</sub> or NH<sub>3</sub> in He). Both physically adsorbed CO<sub>2</sub> and NH<sub>3</sub> were removed by flushing with He (30 mL/min of He) for 10 min before starting recording of the analysis. Lastly, the temperature-programmed desorption was begun following the desorption with both TCD and MS, by increasing the temperature at a constant rate of 10 °C/min from 40/100 to 500 °C in He (30 mL/min). Results were reported and discussed in the ESI (see Figure S2 and accompanying text).

## Results and Discussion

In this Section, we will discuss our results for the energy profile of the mechanism pathways for the dehydration and dehydrogenation of primary and secondary alcohols (see Scheme 1 for the

complete list) in presence of  $\text{Ga}_8\text{O}_{12}$ . The catalytic tests and DRIFT spectra on the lightest species (methanol, ethanol, 1- and 2-propanol) considered in the theoretical analysis are also introduced. We shall start our presentation from the shortest chain ones (i.e. methanol and ethanol), moving up in structural complexity to alcohol containing longer or branched aliphatic chains and unsaturated groups (e.g. aromatic 1-phenyl ethanol or allylic alcohol). We included the latter in order to investigate the possible effect of conjugation or iper-conjugation on the intermediates or the transition state energies. For the lightest species considered in our theoretical analysis, we shall also discuss the results of the complementary experimental studies together with their energy profile, aiming at their complete characterization as well as a robust validation of the theoretical methodology employed for our structure/properties analysis. Experimental data on the reactivity of benzyl alcohol are also provided in the ESI (see Figure S8).



**Scheme 1.** Alcohols used in the theoretical and experimental studies on dehydrogenation and dehydration process.

### 1. Methanol dehydrogenation and ethanol dehydrogenation/dehydration pathways.

Stationary points on the energy surface calculated at DFT level with the B3LYP/6-31+G(d,p) basis set for methanol dehydrogenation and ethanol dehydration and dehydrogenation processes catalysed by  $\text{Ga}_8\text{O}_{12}$  are shown in Table 1 and Figure 1.

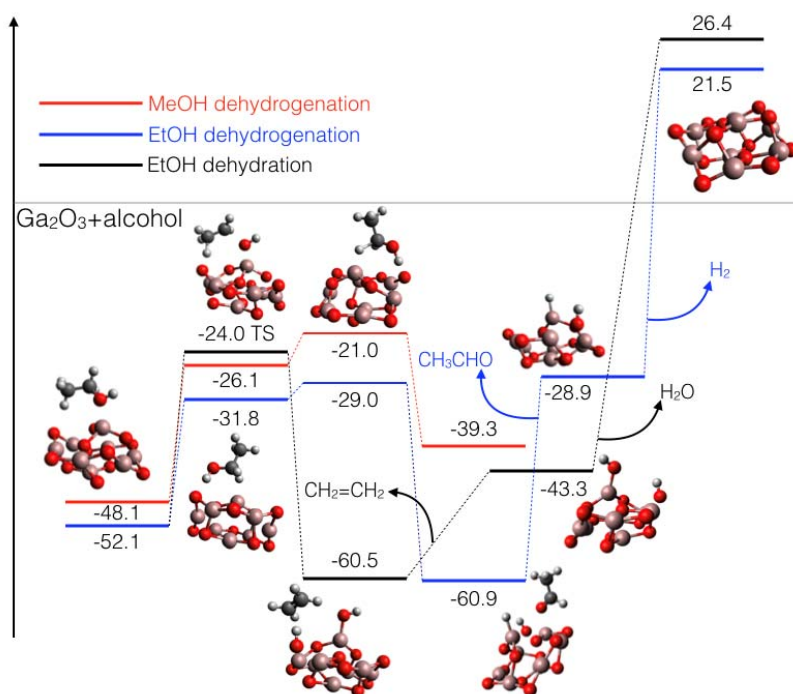


**Figure 1.** Potential energy surfaces for ethanol dehydration and dehydrogenation reactions on  $\text{Ga}_2\text{O}_3$ .

	$\Delta\Delta E(\text{TS})$	Dehydrogenation		Dehydration	
Alcohol	$(E_{\text{deH}_2\text{O}} - E_{\text{deH}_2})$	ads	TS	ads	TS
methanol	---	-26.1	-21.0	-48.1	
ethanol	5.0	-31.8	-29.0	-52.1	-24.0
1-propanol	6.1	-34.6	-31.8	-58.2	-25.8
2-propanol	4.1	-36.5	-34.0	-60.0	-29.7
2-Me-propanol	6.3	-37.0	-34.2	-60.9	-27.9

2-butanol	2.0	-37.3	-35.5	-63.0	-33.4
1-propenol	13.3	-33.2	-31.8	-68.1	-18.9
Benzyl alcohol	---	-41.3	-37.7	-69.7	
1-phenylethanol	-9.24	-44.5	-40.7	-73.1	-49.9
2-phenylethanol	0.25	-58.1	-38.3	-71.2	-38.1

**Table 1:** relative energetic location of the kinetically relevant stationary points describing the dehydrogenation and dehydration pathways (in kcal/mol). The zero of the energy scale is set as the energy of the gas-phase alcohol and gallia cluster. Also, shown, there is the barrier difference ( $\Delta\Delta E(\text{TS})$ ) between the TS's of the two reactive channels.

Considering in detail the overall pathways in presence of  $\text{Ga}_8\text{O}_{12}$ , the first step of mechanism for both the reactions is the adsorption of the reacting alcohol on the cluster, as previously discussed in Refs. [8], [27]. Compared to an energy zero defined as having the two moieties separated, this process leads to a minimum of energy of -48.1 and -52.1 kcal/mol for methanol and ethanol, respectively; this indicates the formation of a strong Lewis acid-base donor-acceptor complex (see Figure 2A for the case of ethanol), which appears to be stabilized by the presence of a longer alkyl chain. Such a complex is characterized by a length of the donor-acceptor bond, meaning the oxygen of the hydroxyl group and the tri-coordinated gallium, of 1.97 and 1.95 Å for methanol and ethanol, respectively, which could be compared with the Ga-O distance within the cluster of about 1.81 Å. A slightly larger difference was found when comparing the Al-O bond of the corresponding Lewis acid-base complex (1.89 Å) with the one present in the  $\text{Al}_8\text{O}_{12}$  cluster (1.71 Å); in addition, the complex of ethanol with gallium is more strongly bound than the one with aluminium (-43.3 and -49.8 kcal/mol at the B3LYP/DZVP2 and CCSD(T)/aug-cc-pVDZ//

B3LYP/DZVP2 levels, respectively[27], the former being in good agreement with B3LYP/6-31+G(d,p) results in Table S4 of the ESI), and of the same complex discussed in Ref. [8] (-36.2 kcal/mol employing the same DFT functional and the 6-311G\* basis set). The latter difference is mainly due to the juxtaposition between the cluster distortion mentioned previously and the somewhat smaller basis set, which may present slightly higher intramolecular basis set superposition errors leading to bond energy overestimation[41].

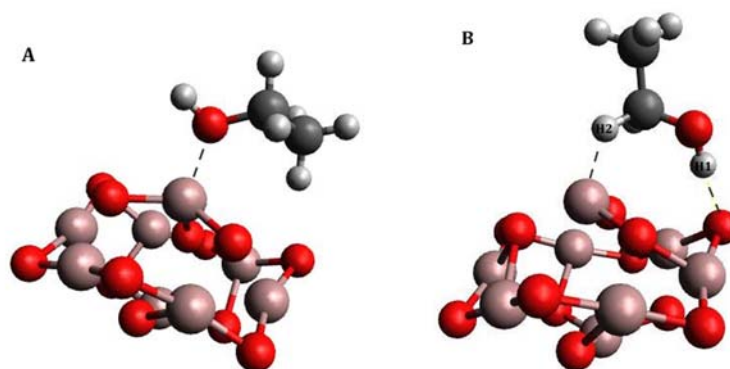


**Figure 2.** Cluster models of  $\text{Ga}_8\text{O}_{12}$  with ethanol adsorbed to form (A) a Lewis acid-base donor (hydroxyl-oxygen)-acceptor (tri-coordinated gallium) bond; and (B) an adduct involving the interaction between the hydroxyl hydrogen and  $\alpha$ -hydrogen and, respectively, a two-coordinated oxygen and the vertex gallium sites on  $\text{Ga}_8\text{O}_{12}$ .

Turning back to dehydration pathway in presence of  $\text{Ga}_8\text{O}_{12}$ , the  $\beta$ -H transfer to an O atom of the cluster to produce ethylene has a barrier energy of 28.1 kcal/mol, and a distance of the  $\beta$ -H to the closest (bi-coordinated) oxygen in the cluster of 1.33 Å at the TS geometry (2.20 Å at the minimum). Comparing with the same reaction pathway in presence of  $\text{Al}_8\text{O}_{12}$ , we notice that energy barriers are similar (namely, 27.0 and 30.1 kcal/mol at the B3LYP/DZVP2 and CCSD(T)/aug-cc-pVDZ//B3LYP/DZVP2 levels, respectively[27]), while the  $\beta$ -CH---O distance is longer over alumina (1.40 Å). We suspect this result to be related to lower atomic charge of the oxygen in the alumina cluster compared to the gallia ones, which is in turn due to the higher Al(III)

acidity. Incidentally, notice that the relative barrier heights on alumina and gallia obtained at the DFT level are in very good agreement with the relative propensity (from 5:1 to 9:8 upon increasing T in the interval 423-523 K) to produce propene from 2-propanol by the two oxides previously discussed[24] (*vide infra* for further discussion on 2-propanol); the latter is instead at variance with the data presented by Kostetskyy and Mpourmpakis[8], which computed a substantially higher TS barrier (roughly, 37.7 kcal/mol) for the dehydration pathway on gallia than on alumina; this would imply a much higher activity toward olefin production by alumina and it was the original thrust to extend the exploration of the reactivity of gallia toward alcohols.

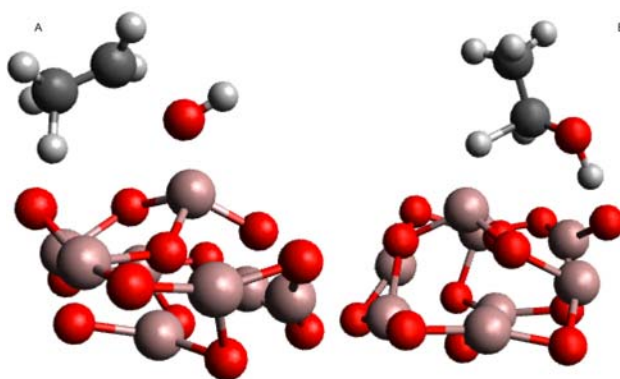


Figure 3: TS's of ethanol leading (A) to dehydration and (B) dehydrogenation on  $\text{Ga}_8\text{O}_{12}$ .

The alternative pathway for alcohol reactivity over gallia leads to formaldehyde and acetaldehyde formation through the dehydrogenation process; albeit it may also be considered to begin from the same Lewis acid-base complex as dehydration, its profile presents a second energy minimum located just before the transition state is reached, and predicted to be at -26.1 and -31.8 kcal/mol, respectively. In this case, the minimum of energy corresponds to a specie interacting with the hydrogen of the hydroxyl group to a two-coordinated peripheral oxygen ( $\text{O}_2$ ) in the cluster (Figure 2 B), and an  $\alpha$ -H atom interacting with the tri-coordinated vertex gallium. The bond length between H and O was predicted to be around 1.7 Å, while the distance between H and Ga(III) was roughly 1.8 Å for both alcohols. The equivalent structure formed by ethanol in presence of  $\text{Al}_8\text{O}_{12}$



has energy of -31.4 kcal/mol, i.e. 0.4 kcal/mol higher than in the presence of gallium. From this point, acetaldehyde is produced by a single step concerted mechanism of transfer of the hydroxyl proton to the cluster rim oxygen and of  $\alpha$ -H atom to the metal cation. Interestingly, the dehydrogenation process catalysed by  $\text{Ga}_8\text{O}_{12}$  has an energy barrier predicted to be 23.0 kcal/mol with respect to the Lewis complex, i.e. 5 kcal/mol lower than the energy barrier calculated for the dehydration reaction (28 kcal/mol). Thus, the relative height of energy barriers for the two pathways on gallia are inverted in to the case of aluminium-based cluster, where the formation of ethylene is more likely than the production of acetaldehyde, with a barrier difference of 5.4 kcal/mol in favour of the former. This latter conclusion appeared in good agreement with the experimental results by Bhan and co-workers[6], which clearly showed a substantial selectivity of alumina toward olefin productions rather than acetaldehyde.

The mechanism of both processes (see energy profiles in Figure 1 for a graphical representation), as obtained following the minimum energy path from the relevant TS, involved the formation of the dehydrogenated or dehydrated products, which remain physisorbed on the gallia cluster. The latter now also bears either the proton/hydride or proton/hydroxide fragments eliminated from the original alcohol. Interestingly, we notice that ethene remains coordinated via its double bond to the proton bound to the oxygen on the cluster edge, while the oxygen of acetaldehyde coordinates with an edge Ga(III). As for this, the results for the dehydrogenation process deviates slightly from what found for alumina[27], as the aldehyde remains coordinated to the proton eliminated in the latter case; besides, the species obtained in both cases are lower in energy than Lewis complex between ethanol and the vertex Ga(III). Detaching acetaldehyde and ethene from the gallia clusters bearing the eliminated species costs, respectively, 32.9 and 17.2 kcal/mol, an energy request somewhat larger than in the alumina case due, probably, to the lightly smaller basis set employed

and, for acetaldehyde, to the Ga(III) interaction. The subsequent loss of H<sub>2</sub> and H<sub>2</sub>O from the remaining clusters requires, respectively, 40.5 and 60.7 kcal/mol. All in all, both the dehydrogenation and dehydration processes appear endothermic (21.5 and 26.4, respectively), as it would be expected basing on simple organic chemistry reactivity.

Noticing the opposing preferred reactivity of ethanol on alumina and gallia emerging from our theoretical calculations and the literature suggestion for gallia to be a good dehydration catalyst for a few alcohols[25], we turned to reactivity experiments to verify whether or not our theoretical conclusions are indeed robust as these may depend on the details of the modelling methodology. As a first approach to this test, methanol was thus continuously fed inside the reactor at 400°C (673 K) in order to evaluate the catalytic activity of gallium oxide for the dehydrogenation reaction of alcohols. The catalytic results are shown in Figure 4. Interestingly, at 400°C Ga<sub>2</sub>O<sub>3</sub> show a very high catalytic activity leading to a methanol conversion of about 95% for 160 minutes of time on stream. A slight deactivation of the catalyst can be seen in both methanol conversion, which decrease from 98 to 95%, and yields into the main reaction products. Indeed, the main products are hydrogen (yield of around 60%), dimethyl ether (DME, ca. 35%), CO<sub>2</sub> (ca. 25%) whose yields slight increase during the time on stream at the expense of CO, the yield of the latter decreasing from 25% to 17%. Noteworthy, two main reaction pathways can be observed over Ga<sub>2</sub>O<sub>3</sub> (Scheme 2, Methanol). The main one is the dehydrogenation of methanol to formaldehyde, which rapidly undergoes to decomposition leading to the formation of CO and hydrogen. Formaldehyde could also undergo disproportionation forming methyl formate that further decomposes leading to the formation of methane (observed in traces) and CO<sub>2</sub>. Another important contribution of the observed reactivity is due to the condensation reaction which lead to the formation of DME and

water. Interestingly, water was observed only in traces (yield below 0.6%) suggesting the presence of the water gas shift reaction (WGS)[14], [42][43].

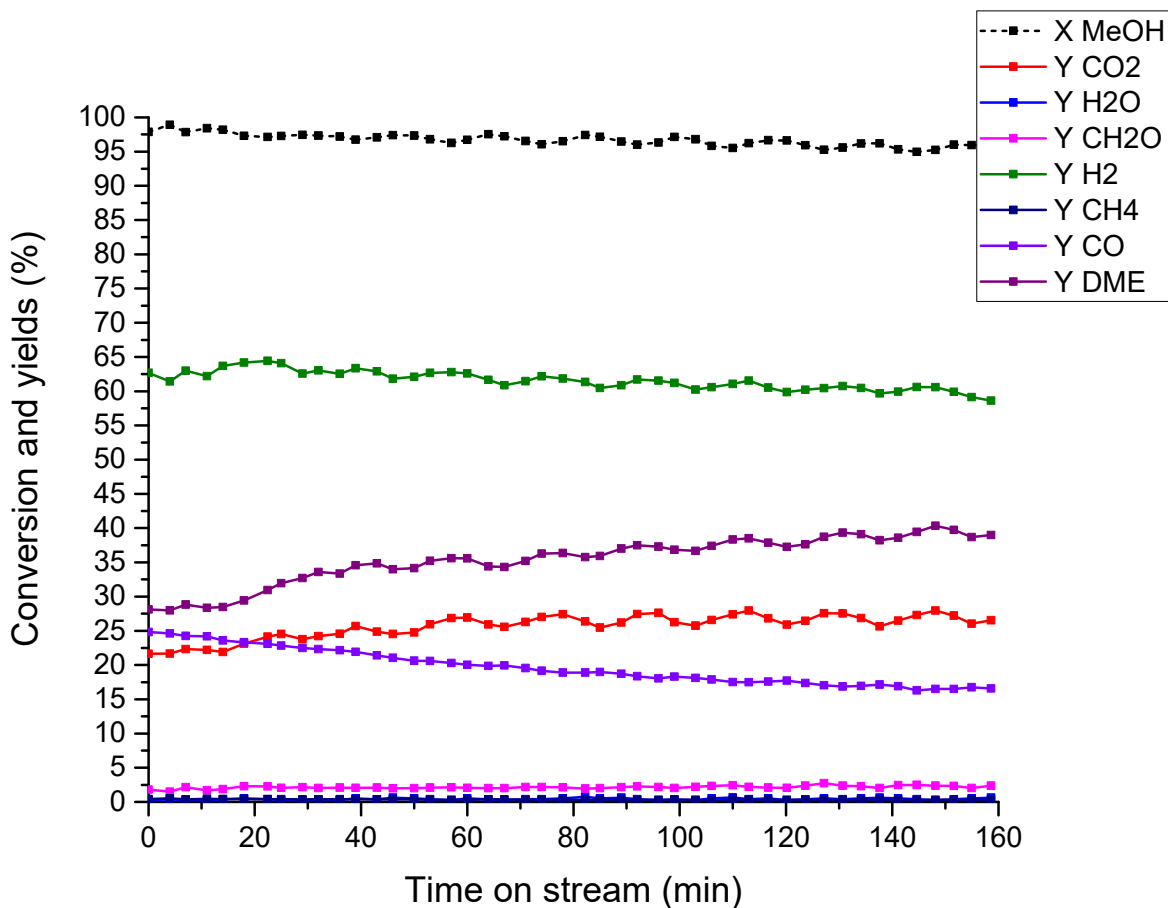


**Figure 4:** Methanol decomposition over Ga<sub>2</sub>O<sub>3</sub> at 400°C,  $\tau=1$ s, feed composition (CH<sub>3</sub>OH:N<sub>2</sub>=18:82)

Turning to ethanol reactivity, our test proved that Ga<sub>2</sub>O<sub>3</sub> is highly active also toward the conversion of this longer chain alcohol. However, a slight progressive deactivation was observed during 200 minutes of time of stream (Figure 5). Similarly to methanol, ethanol undergoes a dehydrogenation leading to the formation of acetaldehyde and hydrogen. Importantly for our testing purpose, ethylene has been observed with a yield of only roughly 8%, demonstrating that the dehydration

of ethanol over the acid sites of gallia is, indeed, a feasible reaction, but also that is less active than dehydrogenation (roughly 35%). Moreover, the intramolecular dehydration is favoured compared to the condensation reaction which would lead to the formation of DEE (ca. 2%). Interestingly, neither the formed ethylene nor DEE can explain the considerable amount of water formed, a clear indication of the presence of consecutive reaction on acetaldehyde (e.g. aldol condensation, dehydration), which lead to the formation of heavier by-products not detectable by our analytical setup (Scheme 2, ethanol). Besides, the formation of ethyl acetate and methyl formate in detectable quantities suggests that gallia may also foster the dehydrogenation of hemiacetals, probably produced via the attack of an alcohol molecule to a Ga(III)-coordinated aldehydes, to esters as done by MgO[10].

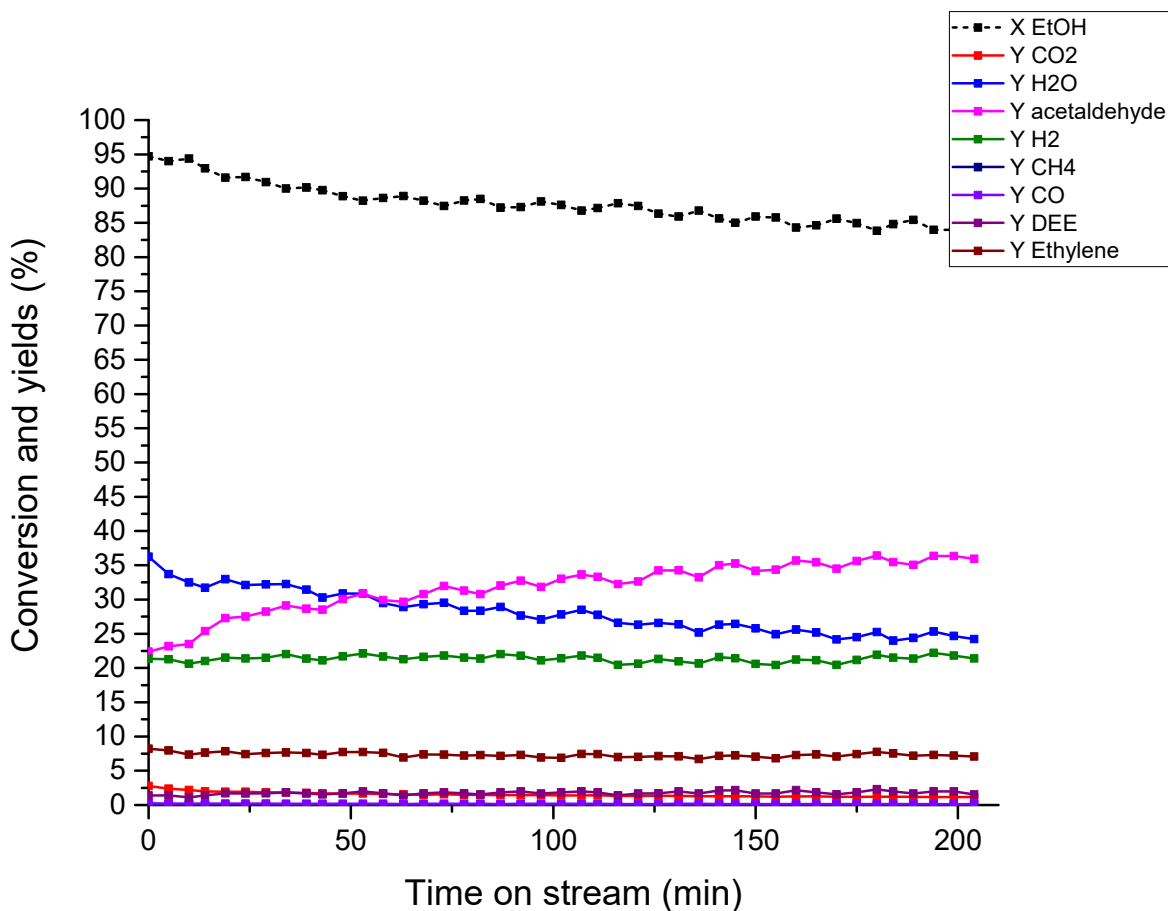
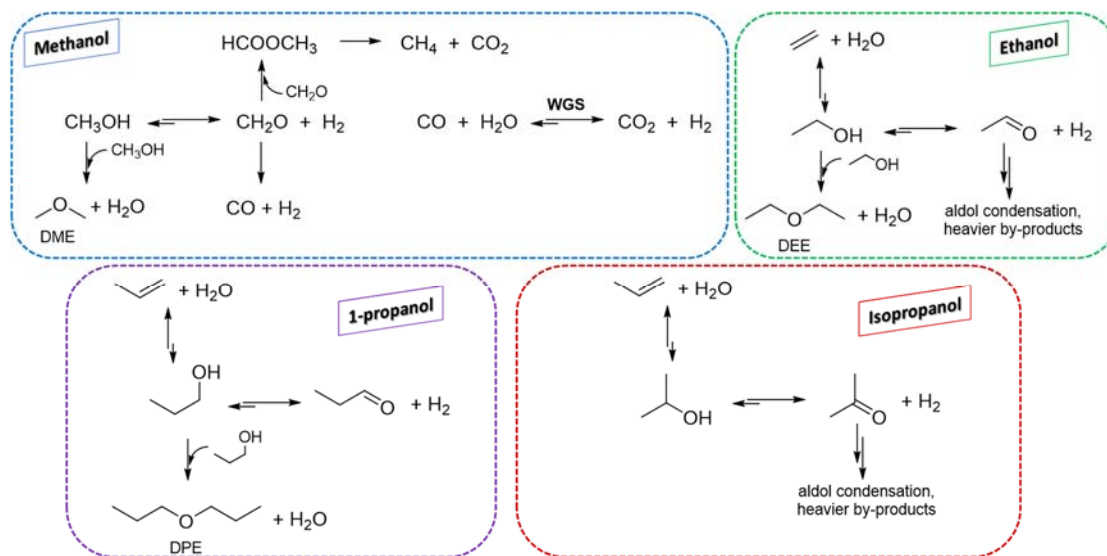


**Figure 5:** Ethanol decomposition over  $\text{Ga}_2\text{O}_3$  at  $400^\circ\text{C}$ ,  $\tau=1\text{s}$ , feed composition (Ethanol: $\text{N}_2=15:85$ ). Other by-products, such as ethyl acetate, 1-butanol, acetone, have been detected with yield  $<2\%$ .



**Scheme 2:** Representation of processes evidenced feeding C1-C3 aliphatic alcohols on gallia.

In concluding this Section, we emphasize that our initial catalysis tests on low mass alcohols indicate the theoretical predictions as being, indeed, quite accurate in terms of relative reactivities, thus suggesting that the theory level exploited may be used to explore the reactivity on gallia of more complicate alcoholic species. This conclusion is made particularly robust by the fact that the results shown in Figures 4 and 5 are for processes that are under a kinetic regime (see Figure S3 in the ESI for data supporting such inference). *De facto*, the possibility that the condensation of acetaldehyde molecules may take place (catalysed by the acid sites present over the catalytic surface) forming heavier compounds and subtracting our detectable products, indeed suggests that our theoretical prediction for the relative reactivity ought to overestimate the experimental results, even though this should be ascribed to the presence of further reactivity for the produced aldehydes (e.g. aldolic condensation or hemiacetal oxidation) on gallia.

### 2.1- and 2-propanol dehydrogenation/dehydration pathways.

We selected to study isomeric 1-propanol and 2-propanol as a way of investigating the impact of a longer chain (comparing with ethanol) or of the secondary nature of an alcohol on the relative reactivity induced by gallia, the theoretical results being shown in Table 1. Notice that, given the relative energetic reported, the shape of the energy profile for both C3 alcohols are indeed similar to the one for ethanol, apart from obvious slight differences in the relative location of local minima and TS's. In fact, both the global and local minima, as well as the TS's for the two processes involving the C3 alcohols are energetically located a few kcal/mol lower with respect to the same stationary points involving ethanol, a finding that may have been expected simply basing on the higher polarizability of the heavier alcohols and/or the stronger inductive effects of the alkyl substituents. The second effect may also be responsible for the slightly lower energetic location for all stationary points involving 2-propanol compare to the 1-propanol case.

Turning to the relative reactivity between dehydrogenation and dehydration, the DFT results suggest the former channel to be the preferred one for both alcohols, with a difference in the respective energies of 6.1 and 4.2 kcal/mol for 1- and 2-propanol, respectively. Compared to ethanol ( $\Delta\Delta E = 5.0$  kcal/mol), the relative preference of the two C3 alcohols toward dehydrogenation can be rationalized easily if one realizes that, i), the dehydration TS resembles a carbocation[4], [8] that requires a lower energy barrier to be surmounted the more the positive charge bearing carbon is substituted, and, ii) the dehydrogenation TS should not be strongly influenced by the number of alkyl substituents on the incipient carbonyl group. The last idea is, *de facto*, supported by the nearly identical value for the energy gap between the global adsorption minimum and the dehydrogenation TS for all alcohols discussed in this and the previous sections.

The reactivity tests (Figures 5 and 6) substantially support the DFT predictions also in the C3 alcohol cases. Thus, despite the fact that increasing the aliphatic chain length of the primary alcohol leads to a significant decrease of the reactivity (the total conversion oscillates around 70% and it is stable for roughly 100 min of time on stream), the main reaction is, by large, the dehydrogenation to propanal (Figure 5). Evidently, also the dehydration to propylene and the condensation reaction to DPE are observed. As in the ethanol case, the excess of water suggest the presence of consecutive side reactions, which lead to the formation of heavier by products; in particular, an off-line GC-MS analysis has indicated the formation of unsaturated C6 compounds, so that the dehydrogenation/dehydration reactivity ratio computed from the results in Figure 6 ought to be an underestimate of the real relative amount of propanal and propene produced.

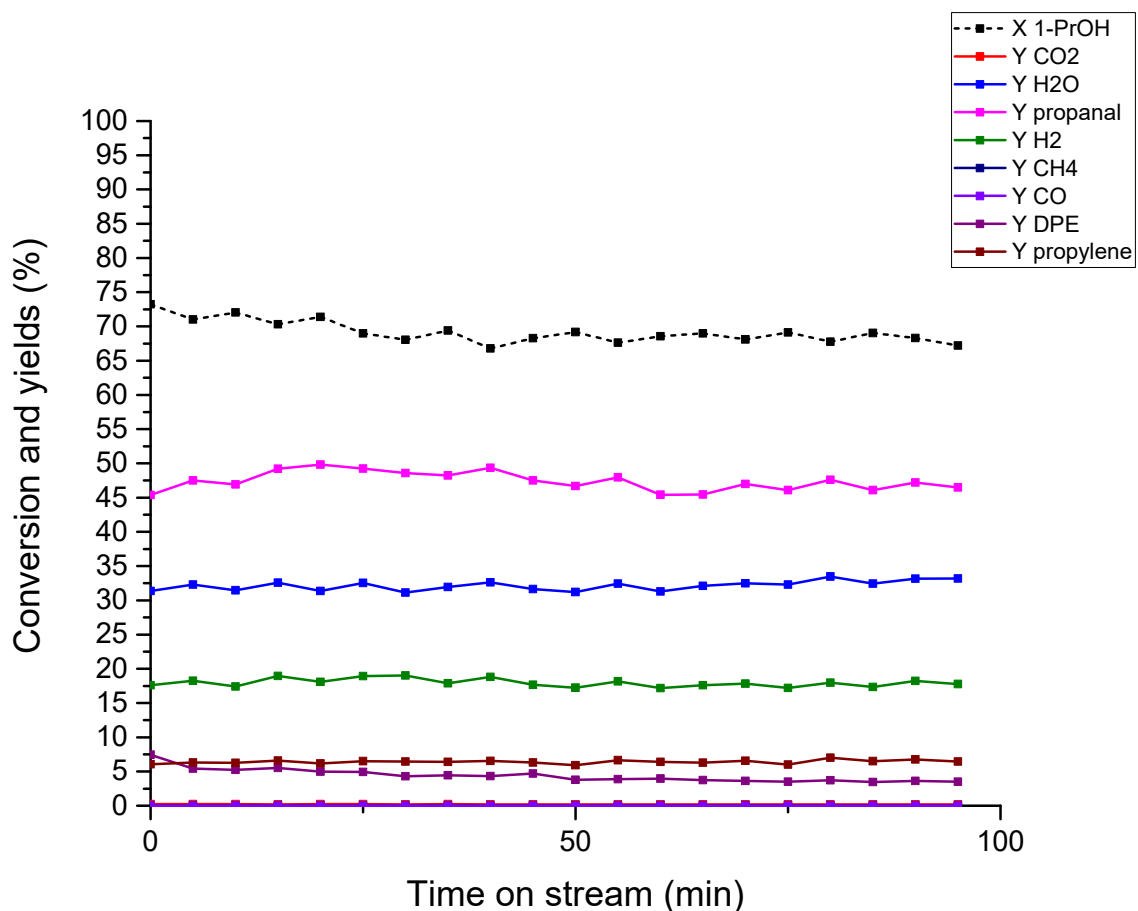


**Figure 6:** 1-propanol decomposition over  $\text{Ga}_2\text{O}_3$  at  $400^\circ\text{C}$ ,  $\tau=1\text{s}$ , feed composition (1-propanol: $\text{N}_2=12:88$ ).

When the secondary alcohol is fed to the reactor, a much higher reactivity is observed. As a matter of fact, a complete and stable isopropanol conversion has been obtained at  $400^\circ\text{C}$  for at least 200 min of time on stream (Figure 7). During this time, both the dehydrogenation (to acetone) and dehydration (to propene) reaction pathways can indeed be observed; albeit the former still remains the most likely reaction (as previously indicated[23], [24]), the relative preference between the two channels appears substantially reduced compared to ethanol and 1-propanol as the DFT results suggested. Besides, we notice the formation of a nearly equimolar amount of water



and propylene, a finding at variance with what recorded for the primary alcohols, and suggesting that ketone or 2-propanol condensation to, respectively, C6 compounds or di-isopropyl ether should be quite limited. This latter suggestion, as well as the general preference for gallia toward the dehydrogenation of 2-propanol, agrees well with the data presented in Ref. [24], thus reinforcing our conclusions on the validity of the modelling approach.

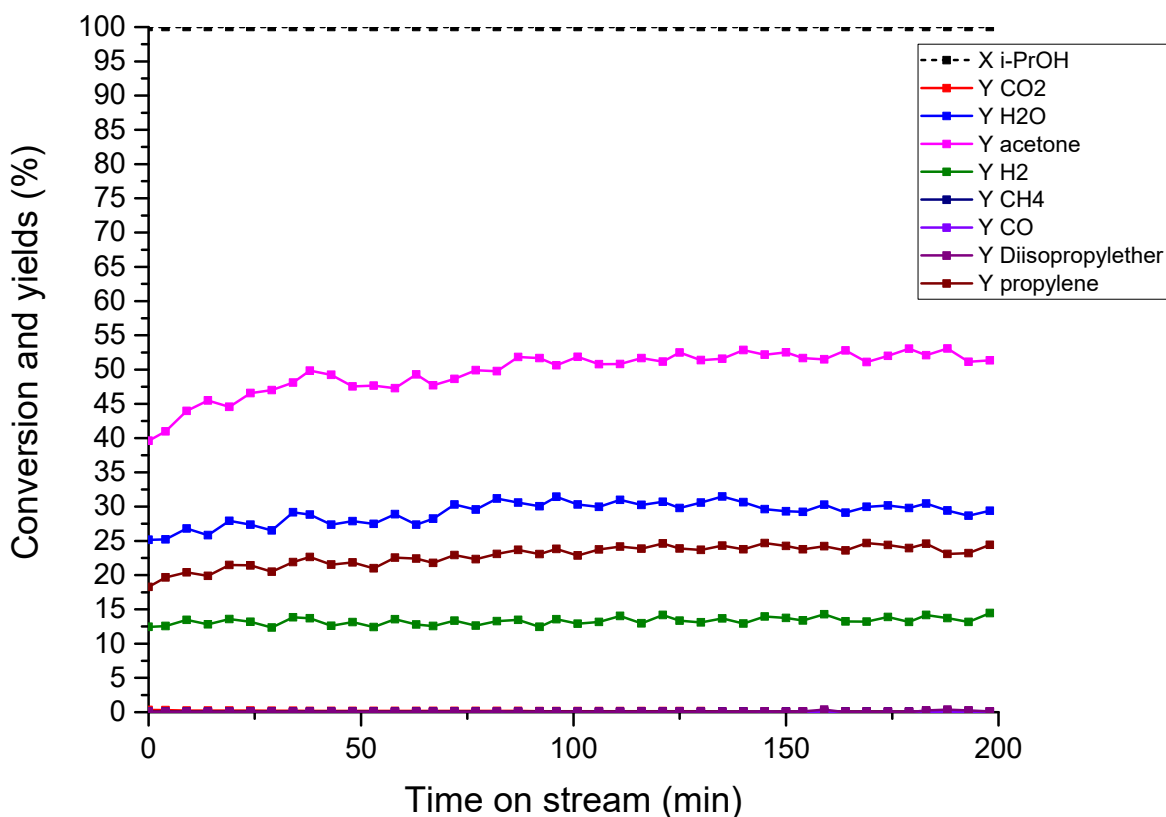


**Figure 7:** 2-propanol decomposition over  $\text{Ga}_2\text{O}_3$  at  $400^\circ\text{C}$ ,  $\tau=1\text{s}$ , feed composition (2-propanol: $\text{N}_2=16:84$ ).

With the aim of improving our understanding regarding the reaction pathways followed by the alcohols over  $\text{Ga}_2\text{O}_3$ , 1-propanol and 2-propanol were also used as representative probes for

primary and secondary alcohols, and their reactivity was studied by DRIFT. To build a more complete understanding, a mass spectrometer was connected to the outlet stream in order to analyse products evolving during the temperature ramp. For the sake of comparisons, propanal, 2-propanone and propylene were studied in the same way, the results of such experiments being reported in the Electronic Supporting Information file (Figures S4-S6).

In discussing DRIFT results, let us begin from 1-propanol, for which, following a gallia pre-treatment at 450°C for 5 hours under He flow, a small amount diluted in He was fed as a pulse to the catalyst at 50°C; spectra were subsequently acquired at 0.5 min time intervals in order to monitor the adsorption profiles. Temperature was then increased until it reached 450°C, with spectra being recorded every 50°C. In figure 8a and 8b, we report the spectra relative to the adsorption of 1-propanol at 50°C together with the spectrum of free alcohol and pre-treated Ga<sub>2</sub>O<sub>3</sub>.

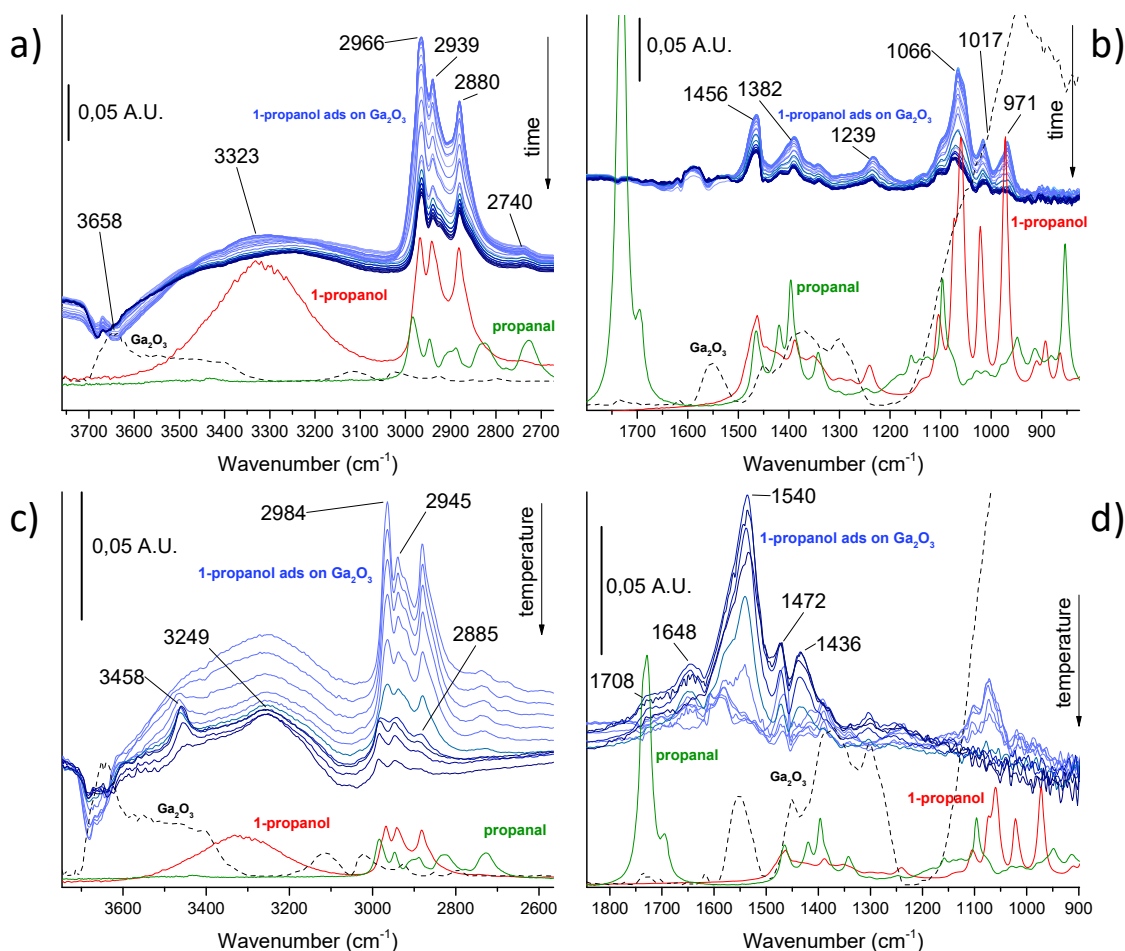


**Figure 8:** DRIFTS spectra of 1-propanol over  $\text{Ga}_2\text{O}_3$ : a) between 3800 and 2600  $\text{cm}^{-1}$  and b) between 1850 and 900  $\text{cm}^{-1}$  during 1-propanol adsorption at 50°C (from azure to blue time elapsed after alcohol pulse; line: red 1-propanol, green propionaldehyde, dotted pre-treated  $\text{Ga}_2\text{O}_3$ ); c) between 3800 and 2600  $\text{cm}^{-1}$  and d) between 1850 and 900  $\text{cm}^{-1}$  during 1-propanol desorption (from azure to blue, spectra recorded from 50°C to 450°C every 50°C; line: red 1-propanol, green propionaldehyde, dotted pre-treated  $\text{Ga}_2\text{O}_3$ ).

The 1-propanol adsorption following the injection pulse produced a fast erosion of the band at  $3658\text{ cm}^{-1}$  attributable to the OH stretching of surface chemisorbed water on  $\text{Ga}_2\text{O}_3$ . The intensity of all the bands increases reaching a maximum corresponding to duration of the pulse; it subsequently decreases reaching a steady state value. In the  $3700 - 2700\text{ cm}^{-1}$  region (Fig. 8a), it is possible to notice the growth of a broad band centred at  $3323\text{ cm}^{-1}$  attributable to the alcohol OH stretching. This band shift toward lower wavenumber during time because of the interaction with gallium oxide surface. Bands at  $2966$ ,  $2939$ ,  $2922$  and  $2880\text{ cm}^{-1}$ , attributable to the CH symmetric and antisymmetric stretching are shifted to higher wavenumber respect to the free 1-propanol due to the interaction with gallia as confirmed by DFT calculations (see Table S2 for the complete attribution helped by DFT based normal mode analysis). Bands relative to the bending (Fig. 8b) match with the free 1-propanol, even though they resulted shifted as happened in the previously discussed spectral region. In particular, the bands attributable to the OH bending at  $1464$  and  $1389\text{ cm}^{-1}$  showed the main shift. Notice that at this temperature, we found no evidence for the formation of any other products; significant differences were, instead, evidenced when temperature was increased. Thus, in the:

- $3700 - 2700\text{ cm}^{-1}$  region (Fig. 8c), the band at  $3323\text{ cm}^{-1}$  evolves in a pair of bands at  $3458$  and  $3249\text{ cm}^{-1}$  attributable to the  $\text{GaO-H}$  and the  $-\text{CO}-\text{H}-\text{OGa}$  stretching respectively. The former may be ascribed to the dehydration of the alcohol to produce propylene, while the latter indicate the strong interaction between 1-propanol and the catalytic surface. Bands attributable to the CH stretching modes decrease with the increase of temperature and shift toward high wavenumber ( $2984$ ,  $2945$  and  $2885\text{ cm}^{-1}$ ). The former could be attributed to the CH stretching of carboxylate species[44].

- 1800 – 1000  $\text{cm}^{-1}$  region (Fig. 8d), bands attributable to 1-propanol bending modes quickly disappear and the concomitant growth of an intense band at 1541, together with the bands at 1708, 1648, 1472, 1436, 1301  $\text{cm}^{-1}$ , was observed. The bands at 1541 and 1436  $\text{cm}^{-1}$  are typical of the asymmetric and symmetric stretching of carboxylate species and the overall spectrum is compatible to the formation of propanoate[44], [45].

Complementarily to pulse adsorption/temperature ramp experiments, continuously feeding 1-propanol in the DRIFT cell at 350°C (Figure 8) made possible to observe the formation of propanal and propylene on the catalytic surface. Thus, the presence of bands ascribable to the propanal could be evidenced (2986, 2730  $\text{cm}^{-1}$ ) in the stretching region (Fig. 9a), together with the couple of OH bends and the CH stretching bands previously described. We found instead impossible to detect the presence of propylene CH stretching bands due to the complexity of the spectra. Its presence is, however, supported by the molecular bending excitations (Fig. 9b), the band at 1650  $\text{cm}^{-1}$  being ascribable to the formation of propylene. In the same region, there are also bands attributable to propanal (1733, 1701, 1472, 1378, 1339, 1300, 1258, 1231  $\text{cm}^{-1}$ ), together with the bands due to propanoate species previously described.

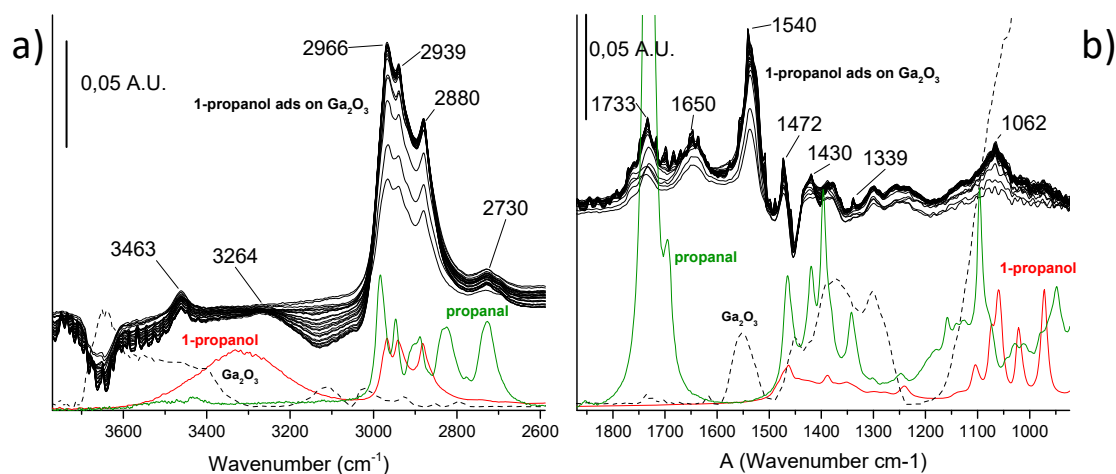


**Figure 9:** *In situ* DRIFTS spectra feeding 1-propanol over  $\text{Ga}_2\text{O}_3$  at  $350^\circ\text{C}$ : a) between  $3800$  and  $2600\text{ cm}^{-1}$  and b) between  $1850$  and  $900\text{ cm}^{-1}$  (line: red 1-propanol, green propionaldehyde, dotted pre-treated  $\text{Ga}_2\text{O}_3$ )

Turning to the DRIFT experiments on 2-propanol over gallium oxides, we begin mentioning that also the interaction of the alcohol with the catalyst during adsorption (Figure 10a and b) produces the erosion of the bands of superficial OH at  $3658\text{ cm}^{-1}$  and the intensity behaviour of the bands related to the 2-propanol are similar to the experiment involving 1-propanol. The band at  $3340\text{ cm}^{-1}$ , due to the OH stretching of free alcohol, quickly shifts toward  $3232\text{ cm}^{-1}$ ; the bands attributable to the stretching modes of the CH strongly decrease after the pulse and, in some cases, resulted shifted compared to the free alcohol, as in case of the bands at  $2971$  and  $2920\text{ cm}^{-1}$  due to the asymmetric and symmetric stretching of  $\text{CH}_3$  that resulted shifted toward higher wavenumbers. When the steady state was reached, the four bands at  $2969$ ,  $2933$ ,  $2920$ ,  $2887\text{ cm}^{-1}$  match with the

respective ones of the free alcohol except for the formation of a new band at  $2872\text{ cm}^{-1}$ , probably ascribed to the CH stretching perturbed by the interaction of the alcoholic group with the catalytic surface (Fig. 10a). In the bending region (Fig. 10b), it is possible to observe bands at 1468, 1413, 1382, 1371, 1341, 1252, 1164, 1132, and  $953\text{ cm}^{-1}$  slightly shifted respect to the free alcohol and attributable to the symmetric and asymmetric deformation of  $\text{CH}_3$  and CO and the stretching of CC (for more detail see ESI, Table S3).

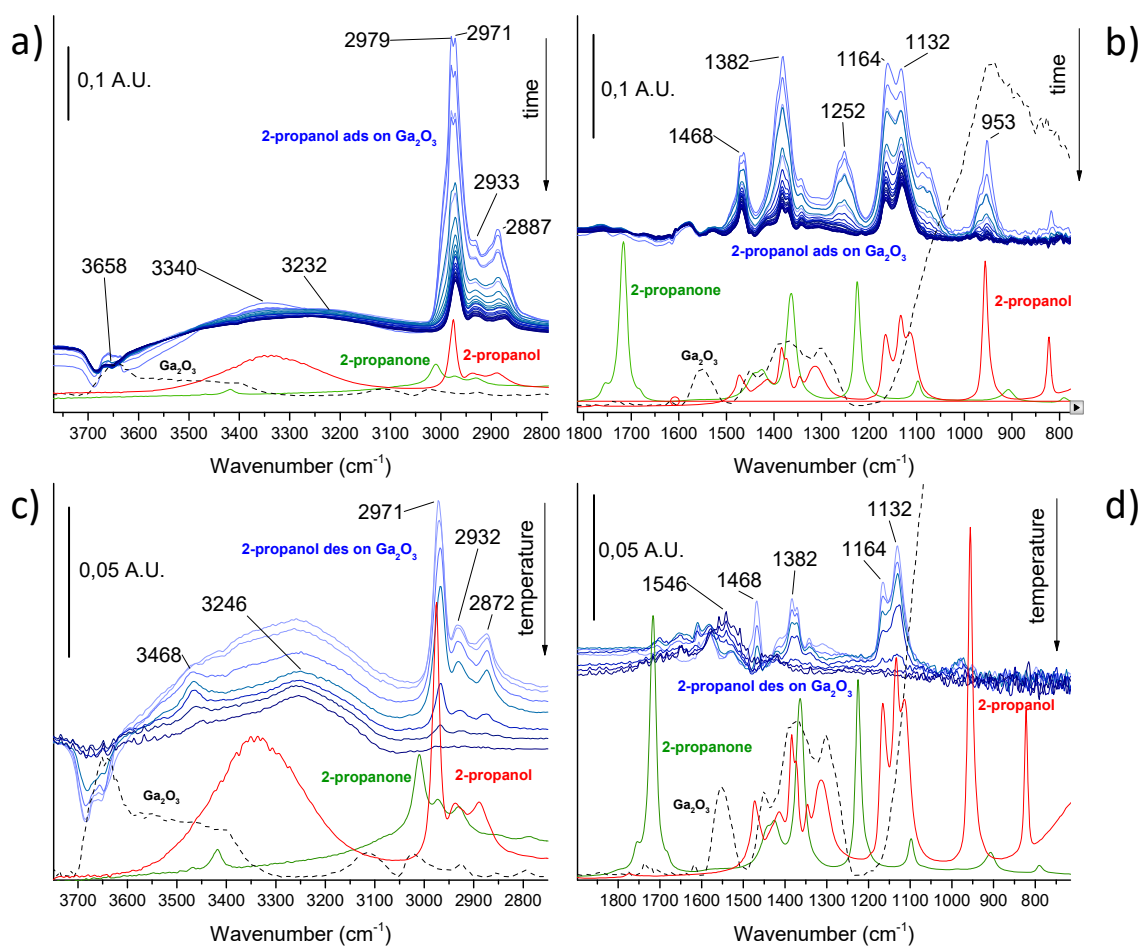


**Figure 10:** DRIFTS spectra of 2-propanol over  $\text{Ga}_2\text{O}_3$ : a) between 3800 and  $2600\text{ cm}^{-1}$  and b) between 1850 and  $900\text{ cm}^{-1}$  during 2-propanol adsorption at  $50^\circ\text{C}$  (from azure to blue time elapsed

after alcohol pulse; line: red 1-propanol, green propionaldehyde, dotted pre-treated  $\text{Ga}_2\text{O}_3$ ); c) between 3800 and 2600  $\text{cm}^{-1}$  and d) between 1850 and 900  $\text{cm}^{-1}$  during 2-propanol desorption (from azure to blue spectra recorded each 50°C from 50°C to 450°C; line: red 2-propanol, green propionaldehyde, dotted pre-treated  $\text{Ga}_2\text{O}_3$ )

During desorption (as induced by a temperature increase), it was possible to observe the formation of a new band at 3468  $\text{cm}^{-1}$  attributable to the GaO-H stretching due to the dehydration of alcohol in the 3700 – 2800  $\text{cm}^{-1}$  region (Fig. 10c); no substantial changes, instead, were observed for the CH stretching bands that decrease upon increasing temperature. In the 1800 – 800  $\text{cm}^{-1}$  region (Fig. 10d), the bands due to the adsorbed 2-propanol progressively disappear upon increasing temperature, and two very low intense bands at 1546 and 1423  $\text{cm}^{-1}$  start to grow. These two bands could be assigned to the hemiacetal species, also observed during 2-propanone adsorption (see ESI, Figure S5)[46].

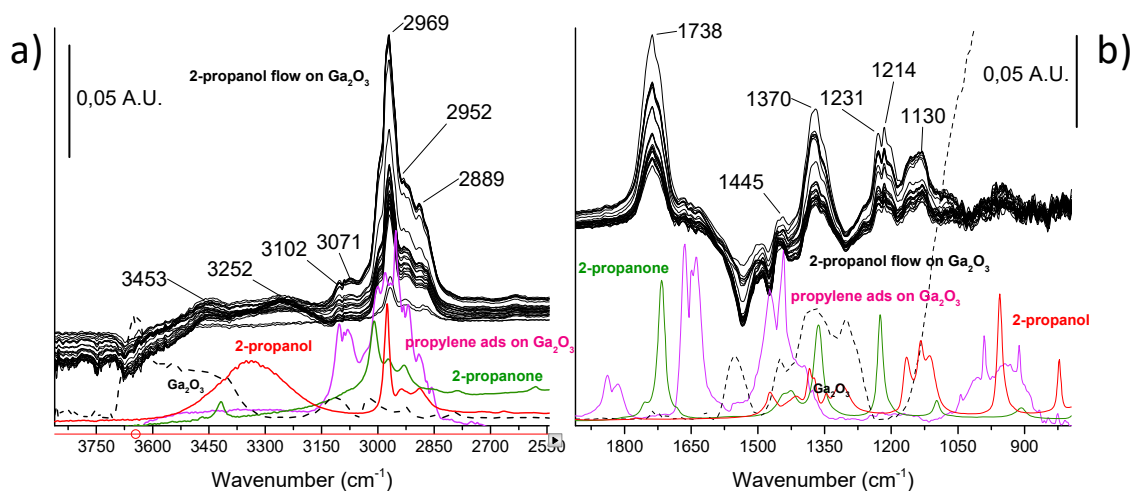




**Figure 11:** *In situ* DRIFTS spectra feeding 2-propanol over Ga<sub>2</sub>O<sub>3</sub> at 350°C: a) between 3800 and 2600 cm<sup>-1</sup> and b) between 1850 and 900 cm<sup>-1</sup> (line: red 1-propanol, green propionaldehyde, dotted pre-treated Ga<sub>2</sub>O<sub>3</sub>)

As with the primary alcohol, the experiment conducted continuously feeding 2-propanol on the catalytic surface at 350°C resulted more helpful for the identification of the reaction products. In Figure 10a, it is possible to prove the evolution of propylene (bands at 3102, 3090, 3080, 3071, 2989, 2980, 2952, 2917, 2889, 2868 cm<sup>-1</sup>), while the bands of acetone, which in this region present a very low intensity, are superimposed to the CH stretching bands of 2-propanol. The pair of broad bands at 3453 and 3252 cm<sup>-1</sup> attributable to the stretching of GaO-H and CO-H of adsorbed 2-propanol, respectively, remain still noticeable. In the bending region (Fig. 10b), bands at 1841, 1665, 1649, 1636 cm<sup>-1</sup> attributable to the C=C stretching and CH bending modes of propylene are noticeable associated with the bands at 1738, 1370 and 1231 cm<sup>-1</sup> due to the presence 2-propanone. For more details regarding the adsorption of both propylene and 2-propanone (see ESI Figures S5 and S6).

Noteworthy, the evolution of substances observed via DRIFT spectroscopy is in good accordance with both the catalytic tests, performed in the continuous flow gas phase reactor, and with the on-line MS connected with DRIFT itself (Figure S7). In particular, comparing the results obtained by feeding 1-propanol and 2-propanol allows one to evidence that: i) the primary alcohol preferentially lead to the formation of propanal through a dehydrogenation pathway, producing propylene as main by-product; ii) the evolution of CO<sub>2</sub> is ascribable to the decarboxylation of propanoate species directly derived from propanal (hence, the dehydrogenation of 1-propanol may

proceed further, albeit it is difficult to indicate if via a direct pathway or involving an hemiacetal);  
iii) feeding 2-propanol lead to a decrease in the acetone/propylene product ratio as reported in Figures 6 and S7.

All in all, the electronic structure modelling employed to pre-investigate the reactivity of the simple primary and secondary alcohols discussed insofar, reactivity tests and *in situ* DRIFT spectroscopy agree well with respect to relative propensity of the dehydrogenation/dehydration reactive channels on gallia. Thus, we shall discuss the theoretical results involving more complicate alcohols with some degree of confidence.

### **3. Dehydrogenation/dehydration pathways for primary and secondary alcohols.**

Spurred by the very good agreement between theoretical prediction of small alcohol reactivity on gallia and the results of both reactivity tests and *in situ* spectroscopy experiments, potential energy surface stationary points were calculated for the dehydration and dehydrogenation pathways catalysed by Ga<sub>8</sub>O<sub>12</sub> for a larger set of primary and secondary alcohols of varying substitutions. Data are shown in Table 1 together with the results previously discussed. Very interestingly, the dehydrogenation process is energetically favourite with respect to dehydration for nearly the totality of the alcohols considered in this work, making thus more robust the idea that a different reactivity is induced by gallia active sites compared to the ones on alumina. More precisely, our theoretical results suggest that the dehydration process was favoured only when the reactive alcohol is 1-phenylethanol,  $\Delta\Delta E$  values being always positive in all the other cases.

As discussed previously for 2-propanol, the rationale for the different behaviour of 1-phenylethanol may easily be found realizing that an important aspect in the competition between the two pathways is represented by the stability of the incipient carbocation that resembles the

structure of the dehydration TS[8]; in the case of 1-phenylethanol, the positive charge bearing carbon is not only of a secondary nature, but it also has a phenyl group as substituent. This is, notoriously, capable of stabilizing charges via resonance between electronic structures (see Figure 12). Indeed, the evidence that most neatly supports this idea, apart from the delocalization over the carbocation of the molecular orbital describing the phenyl  $\pi$  system (Fig. 12, top left), emerges by comparing the dehydration barrier for ethanol and its aromatically substituted counterpart; for the latter, the TS to be surmounted lies nearly 5 kcal/mol closer to the adsorption minimum than for the ethanol case.

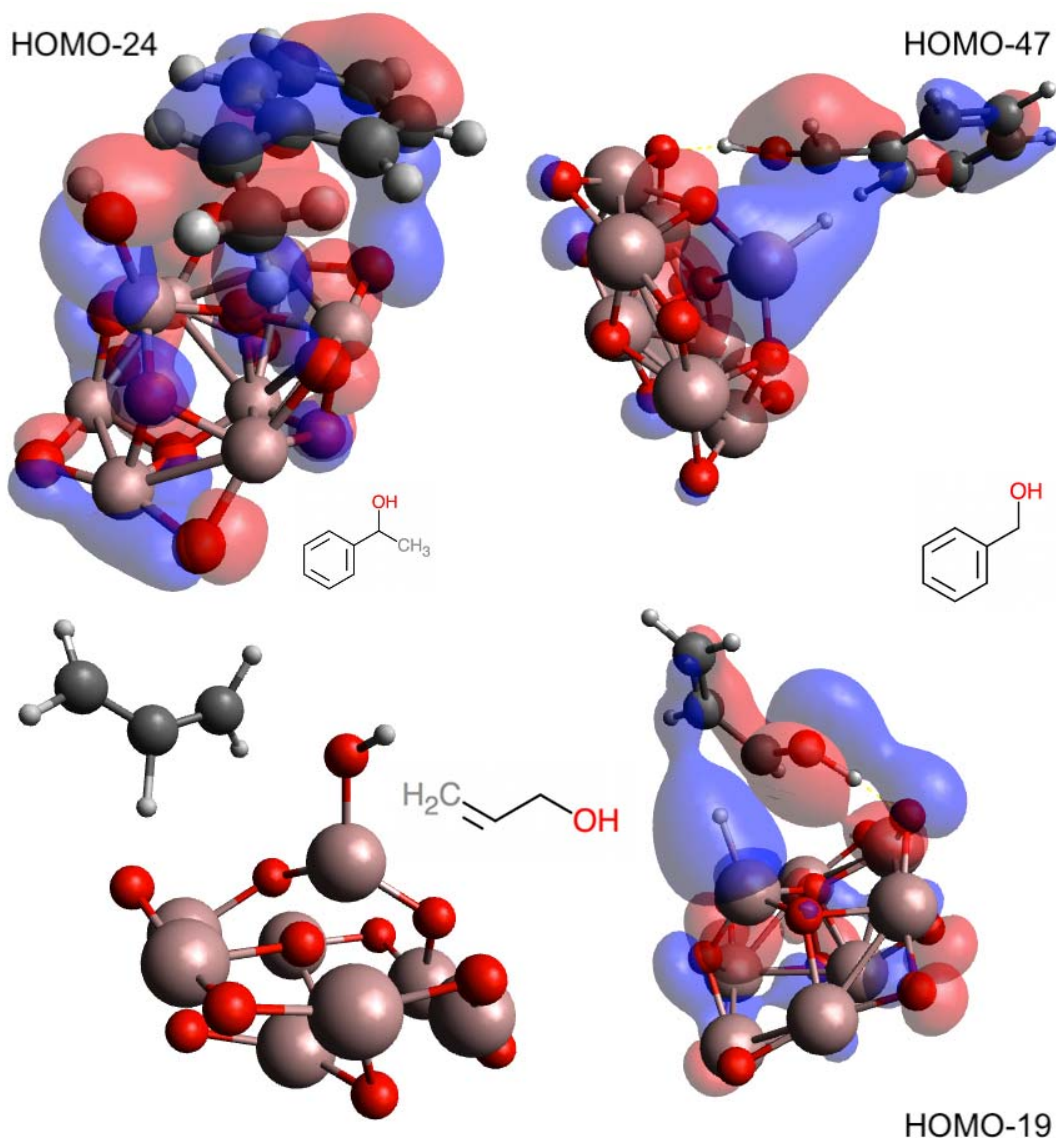


**Figure 12:** TS structures and their stabilizing molecular orbitals for 1-phenyl ethanol dehydration, benzyl alcohol dehydrogenation, and for both processes involving 1-propenol. The energetic location of the shown orbitals is indicated with respect to the system HOMO.

Additional insights on the structure-(re)activity relationship for primary and secondary alcohols interacting with nanostructured gallia may be extracted comparing the energetic location of the stationary points for the two pathways involving the remaining members of our pool of molecular

structures (Table 1). As first comment, let us point out that the relative energy of all the minima is lowered by increasing the complexity (i.e. number and kind of substituents) of the alcohols, a trend that is generally followed also by the TS's for the two competitive pathways. More in the specific, it emerges that adding a methyl substituent in position 2 to 1-propanol should be expected to increase selectivity toward dehydrogenation ( $\Delta\Delta E=6.3$  kcal/mol) due to an increase in the barrier to be surmounted to reach the dehydration TS; in other words, increasing the number of alkyl substituents on the carbon atom that would form the C=C double bond, while leaving the OH-bearing carbon as primary, destabilizes the dehydration TS with respect to the global adsorption minimum. We suggest that this is most likely due to a decrease in the intermolecular interaction strength between the alcohol and the gallia cluster while a Lewis complex reaches the TS geometry (Figure 13).

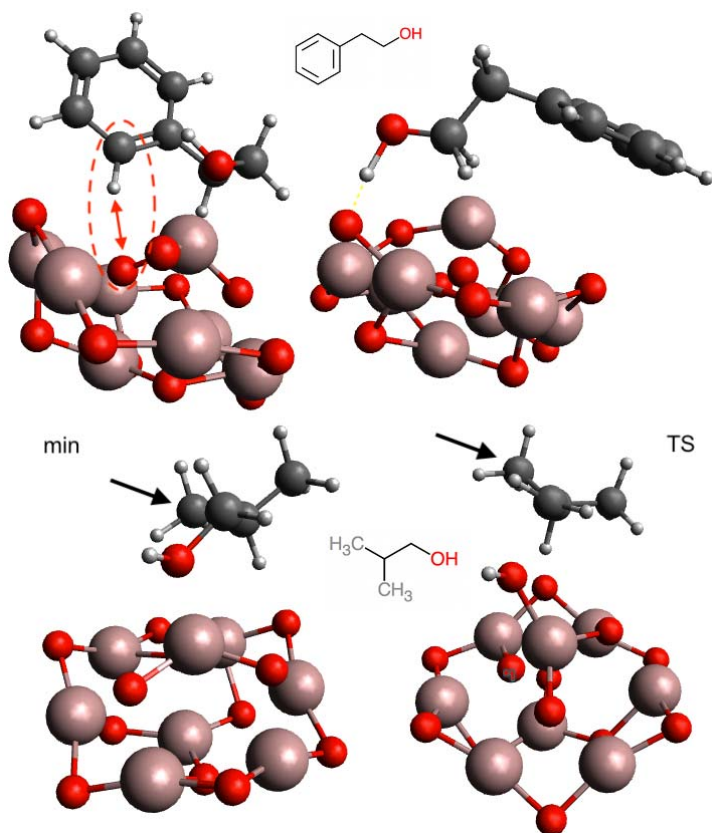


**Figure 13:** Minimum energy (left) and TS (right) structures for the dehydrogenation process involving 2-phenyl ethanol, and the dehydration reaction of 2-methyl propanol. We have evidenced the strong electrostatic interaction between the phenyl ring (red oval) or the methyl substituent (black arrow) of the aliphatic alcohol with the gallia cluster that are cleaved to reach the TS geometries.

At variance with what just discussed, the energy profiles for 2-phenyl ethanol, i.e. the other primary alcohol with a non-conjugable substituent to the OH-bearing primary carbon, suggest that a marked competition between the two reactive channels ought to be present. In this case, however, the rationale for such predictions is found in the fact that more energy is needed to reach the dehydrogenation TS from any of the minima due to the cleavage of the strong electrostatic interaction between the phenyl substituents and  $\text{Ga}_8\text{O}_{12}$  compared to the energy needed to reach the dehydration TS (Figure 13). In other words, the intermolecular interaction between the substituent or chain of an alcohol with the gallia cluster may deeply modify the reaction profile compared to lighter species without involving electronic structure effects such as conjugation or delocalization.

Turning our attention towards the last secondary alcohol, i.e. 2-butanol, one notices that increasing the length of one of the substituents ought to reduce the selectivity of gallia toward dehydrogenation compared to both ethanol and 2-propanol. While such finding may be partially attributable to a stronger inductive effect of the methyl and ethyl substituent on the 2-butanol compared to the two methyl groups in 2-propanol, we highlight also that the former alcohol requires surmounting a higher energy barrier than 2-propanol to reach the dehydrogenation TS

from the global adsorption minimum, which suggests, once again, that gallia-alcohol interactions play a role in the competition between reactive channels.

To conclude our analysis of the energy profiles as a function of the alcohol structures, we notice that 1-propenol ought to present the highest theoretical relative selectivity toward dehydrogenation, the energy gap separating the latter TS from the dehydration one being 13.3 kcal/mol. Such large difference descends primarily from a marked increase in the energy barrier to reach the dehydration TS compared to the dehydrogenation one, this finding being due to the allene-like electronic structure of the dehydration TS (Fig. 12). In fact, apart from the notorious electronic crowding of the two double bonds that increase the average electron repulsion in the final product and TS, the system cannot stabilize the incipient carbocation via conjugation as the  $\pi$  orbital of the double bond initially present is forced into a conformation in which it has zero overlap with the p orbital of the carbon losing the OH group. Besides, the gap between the dehydrogenation TS and the preceding local minimum is reduced compared to both ethanol and 1-propanol, a fact that suggest the involvement of the double bond in the electronic stabilization of the TS. That this is indeed the case, it is shown by the presence of bonding molecular orbitals that delocalize the  $\pi$  orbital of the C=C double bond over the incipient C=O group while also involving the hydride nearly transferred to the Ga(III) active site (see Fig. 12, bottom panel). A similar electronic effect is also present in the dehydrogenation of benzyl alcohol (Figure 12, top panel); in this case, however, the energy gap between the dehydrogenation TS and the closest energy minimum is not as small as for 1-propenol (3.7 kcal/mol), but this is easily justified by realizing that the phenyl substituent is located further apart from the gallia cluster at the TS geometry than in the local minimum structure.

## Conclusions

By means of reactivity tests and *in situ* DRIFTS, we have shown that commercial samples of gallia may be brought to work as dehydrogenation catalyst for short primary and secondary aliphatic alcohols, the latter process being indicated as more active compared to the competing dehydration channel also by DFT calculations. Importantly, the very good agreement between the latter results and experiments robustly validate the modelling approach we exploited. Such conclusion, in turn, allowed us to extend the theoretical study to six more complex archetypical alcohols, five of which are predicted to preferentially undergo dehydrogenation irrespectively of their structural complexity or electronic structure features. Theoretical data also uncovered that the competition between dehydrogenation and dehydration can also be controlled by how the strength of the intermolecular interactions between alcohols and gallia surface differs between low lying adsorbed species and the involved TS's. The behaviour of the only member of our test set of species predicted to preferentially produce an olefin (i.e. 1-phenyl ethanol leading to styrene) was easily rationalized as due to a strong stabilization of the dehydration TS due to conjugation. In view of the weak acidic nature of gallia, its ability to mildly oxidize alcohols may thus pave the way toward the addition of complicate substituents to activated (e.g. phenols[14]) aromatic compounds.

## Electronic Supporting Information.

The following additional data are available free of charge.

Tables of the vibrational frequencies measured via IR spectroscopy and computed by DFT calculations; DRIFTS results for propanal, acetone and propylene adsorbed on gallia (PDF); BET and TPD characterization of the materials; catalytic results for benzyl alcohol; test on the possible diffusion controlled regimes employing ethanol; DFT energy profiles for



dehydrogenation and dehydration of ethanol on alumina; MS spectra recorded during DRIFTS experiments involving 2-propanol.

## CONFLICTS OF INTEREST

There are no conflicts to declare

## ACKNOWLEDGMENT

MM, LI, and CL kindly acknowledge funding from the Fondo d'Ateneo per la Ricerca (FAR2018) dell'Università degli Studi dell'Insubria.

## REFERENCES

- [1] A. Chieregato, J. Velasquez Ochoa, C. Bandinelli, G. Fornasari, F. Cavani, and M. Mella, “On the Chemistry of Ethanol on Basic Oxides: Revising Mechanisms and Intermediates in the Lebedev and Guerbet reactions,” *ChemSusChem*, vol. 8, no. 2, pp. 377–388, Jan. 2015.
- [2] R. Mazzoni *et al.*, “Catalytic Biorefining of Ethanol from Wine Waste to Butanol and Higher Alcohols: Modeling the Life Cycle Assessment and Process Design,” *ACS Sustain. Chem. Eng.*, vol. 7, no. 1, pp. 224–237, Jan. 2019.
- [3] Z. Fang, Y. Wang, and D. A. Dixon, “Computational Study of Ethanol Conversion on Al<sub>2</sub>O<sub>3</sub> as a Model for  $\gamma$ -Al<sub>2</sub>O<sub>3</sub>,” *J. Phys. Chem. C*, vol. 119, no. 41, pp. 23413–23421, Oct. 2015.
- [4] S. Roy, G. Mpourmpakis, D.-Y. Hong, D. G. Vlachos, A. Bhan, and R. J. Gorte, “Mechanistic study of alcohol dehydration on  $\gamma$ -Al<sub>2</sub>O<sub>3</sub>,” *ACS Catal.*, vol. 2, no. 9, pp. 1846–1853, 2012.

- [5] J. F. DeWilde, H. Chiang, D. A. Hickman, C. R. Ho, and A. Bhan, “Kinetics and mechanism of ethanol dehydration on  $\gamma$ -Al<sub>2</sub>O<sub>3</sub>: The critical role of dimer inhibition,” *ACS Catal.*, vol. 3, no. 4, pp. 798–807, 2013.
- [6] J. F. DeWilde, C. J. Czopinski, and A. Bhan, “Ethanol dehydration and dehydrogenation on  $\gamma$ -Al<sub>2</sub>O<sub>3</sub>: Mechanism of acetaldehyde formation,” *ACS Catal.*, vol. 4, no. 12, pp. 4425–4433, 2014.
- [7] M. Kang, J. F. Dewilde, and A. Bhan, “Kinetics and mechanism of alcohol dehydration on  $\gamma$ -Al<sub>2</sub>O<sub>3</sub>: Effects of carbon chain length and substitution,” *ACS Catal.*, vol. 5, no. 2, pp. 602–612, 2015.
- [8] P. Kostestkyy, J. Yu, R. J. Gorte, and G. Mpourmpakis, “Structure-activity relationships on metal-oxides: Alcohol dehydration,” *Catal. Sci. Technol.*, vol. 4, no. 11, pp. 3861–3869, 2014.
- [9] M. A. Christiansen, G. Mpourmpakis, and D. G. Vlachos, “Density functional theory-computed mechanisms of ethylene and diethyl ether formation from ethanol on  $\gamma$ -Al<sub>2</sub>O<sub>3</sub>(100),” *ACS Catal.*, vol. 3, no. 9, pp. 1965–1975, 2013.
- [10] T. Pasini, A. Lolli, S. Albonetti, F. Cavani, and M. Mella, “Methanol as a clean and efficient H-transfer reactant for carbonyl reduction: Scope, limitations, and reaction mechanism,” *J. Catal.*, vol. 317, 2014.
- [11] M. S. Gyngazova *et al.*, “Mechanistic insights into the catalytic transfer hydrogenation of furfural with methanol and alkaline earth oxides,” *J. Catal.*, vol. 372, pp. 61–73, 2019.

- [12] C. Lucarelli *et al.*, “Tandem hydrogenation/hydrogenolysis of furfural to 2-methylfuran over a Fe/Mg/O catalyst: Structure–activity relationship,” *Catalysts*, vol. 9, no. 11, 2019.
- [13] C. Cesari *et al.*, “Hydrogen Transfer Activation via Stabilization of Coordinatively Vacant Sites: Tuning Long-Range  $\pi$ -System Electronic Interaction between Ru(0) and NHC Pendants,” *Organometallics*, vol. 38, no. 5, pp. 1041–1051, 2019.
- [14] T. Tabanelli *et al.*, “Mg/Ga mixed-oxide catalysts for phenol methylation: Outstanding performance in 2,4,6-trimethylphenol synthesis with co-feeding of water,” *Appl. Catal. A Gen.*, vol. 552, 2018.
- [15] T. Tabanelli *et al.*, “A cascade mechanism for a simple reaction: The gas-phase methylation of phenol with methanol,” *J. Catal.*, vol. 370, pp. 447–460, 2019.
- [16] M. Bregolato *et al.*, “Methylation of phenol over high-silica beta zeolite: Effect of zeolite acidity and crystal size on catalyst behaviour,” *J. Catal.*, vol. 245, no. 2, pp. 285–300, 2007.
- [17] T. Tabanelli, S. Passeri, C. Lucarelli, D. Zhambakin, and F. Cavani, “Methanol as the precursor of the true electrophilic reactant in the multi-step methylation of phenolics catalysed by mixed metal oxides: Superior performance of FeVO<sub>4</sub> catalyst,” in *DGMK Tagungsbericht*, 2015, vol. 2015, no. 2, pp. 283–289.
- [18] V. Crocellà *et al.*, “Gas-phase phenol methylation over Mg/Me/O (Me = Al, Cr, Fe) catalysts: Mechanistic implications due to different acid-base and dehydrogenating properties,” *Dalt. Trans.*, vol. 39, no. 36, pp. 8527–8537, 2010.
- [19] F. Cavani, L. Maselli, S. Passeri, and J. A. Lercher, “Catalytic methylation of phenol on

- MgO - Surface chemistry and mechanism,” *J. Catal.*, vol. 269, no. 2, pp. 340–350, 2010.
- [20] N. Ballarini, F. Cavani, L. Maselli, S. Passeri, and S. Rovinetti, “Mechanistic studies of the role of formaldehyde in the gas-phase methylation of phenol,” *J. Catal.*, vol. 256, no. 2, pp. 215–225, 2008.
- [21] N. Ballarini *et al.*, “The transformations involving methanol in the acid- and base-catalyzed gas-phase methylation of phenol,” *J. Catal.*, vol. 251, no. 2, pp. 423–436, 2007.
- [22] M. Ardizzi *et al.*, “Environmentally friendly, heterogeneous acid and base catalysis for the methylation of catechol: Chances for the control of chemo-selectivity,” *Appl. Catal. B Environ.*, vol. 70, no. 1–4, pp. 597–605, 2007.
- [23] H. B. B. Bremer, “Zum Verhalten einiger Modifikationen des Gallium(III)-oxids und -oxidhydrorids als Katalysatoren des Isopropanolzerfalls,” *Z. Chem.*, vol. 7, p. 470, 1967.
- [24] J. N. Díaz de Leon *et al.*, “Catalytic dehydration of 2 propanol over Al<sub>2</sub>O<sub>3</sub>-Ga<sub>2</sub>O<sub>3</sub> and Pd/Al<sub>2</sub>O<sub>3</sub>-Ga<sub>2</sub>O<sub>3</sub> catalysts,” *Catal. Today*, May 2019.
- [25] B. H. Davis, S. Cook, and R. W. Naylor, “Catalytic conversion of alcohols. 8. Gallium oxide as a dehydration catalyst,” *J. Org. Chem.*, vol. 44, no. 13, pp. 2142–2145, Jun. 1979.
- [26] D. Pappalardo, C. Pellecchia, G. Milano, and M. Mella, “Reactivity of a cationic alkyl amino-functionalized cyclopentadienyl aluminum compound with olefins: NMR observation and computational investigation of the single propene insertion product into an Al-C bond,” *Organometallics*, vol. 28, no. 8, 2009.
- [27] Z. Fang, Y. Wang, and D. A. Dixon, “Computational Study of Ethanol Conversion on Al<sub>8</sub>

- O<sub>12</sub> as a Model for  $\gamma$ -Al<sub>2</sub>O<sub>3</sub>,” *J. Phys. Chem. C*, vol. 119, no. 41, pp. 23413–23421, Oct. 2015.
- [28] A. Vimont, J. C. Lavalley, A. Sahibed-Dine, C. Otero Areán, M. Rodríguez Delgado, and M. Daturi, “Infrared Spectroscopic Study on the Surface Properties of  $\gamma$ -Gallium Oxide as Compared to Those of  $\gamma$ -Alumina,” *J. Phys. Chem. B*, vol. 109, no. 19, pp. 9656–9664, May 2005.
- [29] J. Ye, C. Liu, D. Mei, and Q. Ge, “Active Oxygen Vacancy Site for Methanol Synthesis from CO<sub>2</sub> Hydrogenation on In<sub>2</sub>O<sub>3</sub>(110): A DFT Study,” *ACS Catal.*, vol. 3, no. 6, pp. 1296–1306, Jun. 2013.
- [30] M. M. Branda, G. R. Garda, H. A. Rodriguez, and N. J. Castellani, “Methanol decomposition on the  $\beta$ -Ga<sub>2</sub>O<sub>3</sub> (100) surface: A DFT approach,” *Appl. Surf. Sci.*, vol. 254, no. 1, pp. 120–124, 2007.
- [31] J. Ye, C. Liu, and Q. Ge, “DFT Study of CO<sub>2</sub> Adsorption and Hydrogenation on the In<sub>2</sub>O<sub>3</sub> Surface,” *J. Phys. Chem. C*, vol. 116, no. 14, pp. 7817–7825, Apr. 2012.
- [32] M. M. Branda, S. E. Collins, N. J. Castellani, M. A. Baltanás, and A. L. Bonivardi, “Methanol Adsorption on the  $\beta$ -Ga<sub>2</sub>O<sub>3</sub> Surface with Oxygen Vacancies: Theoretical and Experimental Approach,” *J. Phys. Chem. B*, vol. 110, no. 24, pp. 11847–11853, Jun. 2006.
- [33] J. C. Lavalley *et al.*, “Unexpected similarities between the surface chemistry of cubic and hexagonal gallia polymorphs,” *Phys. Chem. Chem. Phys.*, vol. 5, no. 6, pp. 1301–1305, 2003.

- [34] A. D. Becke, "Density-functional thermochemistry. III. The role of exact exchange," *J. Chem. Phys.*, vol. 98, no. 7, pp. 5648–5652, Apr. 1993.
- [35] P. J. Stephens, F. J. Devlin, C. F. Chabalowski, and M. J. Frisch, "Ab Initio Calculation of Vibrational Absorption and Circular Dichroism Spectra Using Density Functional Force Fields," *J. Phys. Chem.*, vol. 98, no. 45, pp. 11623–11627, Nov. 1994.
- [36] C. Trevisanut, M. Mari, J.-M. M. Millet, and F. Cavani, "Chemical-loop reforming of ethanol over metal ferrites: An analysis of structural features affecting reactivity," *Int. J. Hydrogen Energy*, vol. 40, no. 15, pp. 5264–5271, Apr. 2015.
- [37] P. B. Vásquez *et al.*, "Gas-Phase Catalytic Transfer Hydrogenation of Methyl Levulinate with Ethanol over ZrO<sub>2</sub>," *ACS Sustain. Chem. Eng.*, vol. 7, no. 9, pp. 8317–8330, May 2019.
- [38] C. Lucarelli *et al.*, "Adsorbent–Adsorbate Interactions in the Oxidation of HMF Catalyzed by Ni-Based MOFs: A DRIFT and FT-IR Insight," *J. Phys. Chem. C*, vol. 120, no. 28, pp. 15310–15321, Jul. 2016.
- [39] L. Grazia *et al.*, "Exploiting H-transfer as a tool for the catalytic reduction of bio-based building blocks: the gas-phase production of 2-methylfurfural using a FeVO<sub>4</sub> catalyst," *Green Chem.*, vol. 19, no. 18, pp. 4412–4422, 2017.
- [40] C. Lucarelli, A. Giugni, G. Moroso, and A. Vaccari, "FT-IR Investigation of Methoxy Substituted Benzenes Adsorbed on Solid Acid Catalysts," *J. Phys. Chem. C*, vol. 116, no. 40, pp. 21308–21317, Oct. 2012.

- [41] A. Ponti and M. Mella, “Three-Fragment Counterpoise Correction of Potential Energy Curves for Proton-Transfer Reactions,” *J. Phys. Chem. A*, vol. 107, no. 38, pp. 7589–7596, 2003.
- [42] C. Lucarelli *et al.*, “Novel Cu-Zn-Al catalysts obtained from hydrotalcite-type precursors for middle-temperature water-gas shift applications,” *Appl. Clay Sci.*, vol. 155, pp. 103–110, 2018.
- [43] D. G. A. Vaccari, C. Lucarelli, N. Schiaroli, G. Fornasari, R. Faure, “WGS,” EP 3 254 760 A1, 2016.
- [44] M. Baldi, F. Milella, G. Ramis, V. Sanchez Escribano, and G. Busca, “An FT-IR and flow reactor study of the selective catalytic oxy-dehydrogenation of C3 alcohols on Mn3O4,” *Appl. Catal. A Gen.*, vol. 166, no. 1, pp. 75–88, 1998.
- [45] C. Resini, T. Montanari, G. Busca, J.-M. Jehng, and I. E. Wachs, “Comparison of alcohol and alkane oxidative dehydrogenation reactions over supported vanadium oxide catalysts: in situ infrared, Raman and UV–vis spectroscopic studies of surface alkoxide intermediates and of their surface chemistry,” *Catal. Today*, vol. 99, no. 1, pp. 105–114, 2005.
- [46] G. Busca, “Infrared studies of the reactive adsorption of organic molecules over metal oxides and of the mechanisms of their heterogeneously-catalyzed oxidation,” *Catal. Today*, vol. 27, no. 3, pp. 457–496, 1996.